cells

MDPI

*Article*

# Resveratrol Modulates High-Fat Diet-Associated Skeletal Muscle Alterations and Extracellular Matrix-Related Transcriptional Responses

**Huibin Zhang [1,2], Qian Li [1], Wenxi Li [1], Hai Jin [1], Xinyi Du [1], Shuanping Zhao [1], Qinggang Li [1], Honglong Zhu [1], Zongjun Yin [2], Xiaodong Zhang [2,*] and Lei Xu [1,*]**

[1] Anhui Provincial Key Laboratory of Livestock and Poultry Product Safety, Institute of Animal Husbandry and Veterinary Medicine, Anhui Academy of Agricultural Sciences, Hefei 230031, China; zhanghuibin1997@126.com (H.Z.)
[2] College of Animal Science and Technology, Anhui Agricultural University, Hefei 230036, China
* Correspondence: xdzhang1983@ahau.edu.cn (X.Z.); xuleirock@163.com (L.X.)

## Highlights

### What are the main findings?

- Concurrent resveratrol intervention increased relative quadriceps weight, altered muscle fibre morphology and modulated inflammatory and oxidative stress-related indices in HFD-fed rats.
- Resveratrol attenuated HFD-associated changes in hydroxyproline content and ECM-related protein concentrations (LOX, MMPs and TIMPs), while exploratory transcriptomics identified 112 candidate genes.

### What are the implications of the main findings?

- ECM-related biochemical and transcriptional responses represent complementary but distinct features associated with resveratrol intervention under HFD conditions.
- The functional significance of the observed morphological alterations and the protein-level and causal roles of individual ECM-related candidate genes require further investigation.

## Abstract

A high-fat diet (HFD) disrupts skeletal muscle homeostasis through metabolic stress, inflammation, oxidative stress and structural alterations. The effects of resveratrol on HFD-associated extracellular matrix (ECM)-related responses remain incompletely characterised. This study evaluated concurrent resveratrol intervention in HFD-fed rats by integrating histomorphological analysis, inflammatory and oxidative stress-related measurements, ECM-related biochemical assessments and exploratory transcriptomics. Resveratrol increased the quadriceps wet weight-to-body weight ratio and altered muscle fibre morphology in HFD-fed rats. Pairwise comparisons of total body weight gain between resveratrol-treated and corresponding untreated groups were not statistically significant, although a significant main effect of resveratrol was detected. Resveratrol attenuated HFD-associated increases in TGF-β1, $H_2O_2$ and MDA and increased IL-10 and T-AOC. HFD feeding increased hydroxyproline, LOX, MMP-2 and MMP-9 levels and MMP/TIMP ratios, while decreasing TIMP-1 and TIMP-2 levels; concurrent resveratrol intervention attenuated these changes. Exploratory transcriptomic analysis identified 112 candidate genes showing opposite expression directions, of which five met the FDR and fold-change

Academic Editors: Gillian Sandra Butler-Browne and Kin Hing William Lau

Received: 18 September 2026
Revised: 17 November 2026
Accepted: 26 November 2026
Published: 28 November 2026

**Copyright:** © 2026 by the authors. Licensee MDPI, Basel, Switzerland. This article is an open access article distributed under the terms and conditions of the Creative Commons Attribution (CC BY) license.

criteria in both comparisons. GO enrichment highlighted collagen fibril organisation and extracellular matrix organisation. RT-qPCR showed concordant expression directions for selected genes, although cross-gene correlations with RNA-seq were not statistically significant. Collectively, resveratrol intervention was associated with morphological alterations and ECM-related biochemical and transcriptional responses in HFD-fed rats. Further protein-level, collagen-specific histological and functional assessments are required to clarify their biological significance.

**Keywords:** resveratrol; high-fat diet; skeletal muscle; oxidative stress; extracellular matrix

## 1. Introduction

Long-term consumption of a high-fat diet (HFD) results in a sustained excess supply of energy and lipids and is an important dietary factor contributing to obesity, insulin resistance and related metabolic disorders [1,2]. Skeletal muscle is a major tissue involved in glucose uptake, fatty acid oxidation and energy metabolism, and can switch between different metabolic substrates according to nutrient availability and energy demand, thereby contributing to the maintenance of whole-body metabolic homeostasis [3,4]. When fatty acid supply chronically exceeds the storage and oxidative capacity of skeletal muscle, intramyocellular lipids and bioactive lipid intermediates, including diacylglycerols and ceramides, may accumulate and subsequently impair insulin signalling and glucose utilisation [2,5]. Meanwhile, HFD feeding can disrupt mitochondrial respiration, fusion–fission balance and mitochondrial quality control in skeletal muscle [6,7], thereby reducing substrate oxidative capacity and increasing reactive oxygen species (ROS) production. These alterations may progressively shift skeletal muscle from metabolic adaptation towards impaired metabolic flexibility and disrupted tissue homeostasis. Therefore, clarifying the pathological basis of HFD-induced skeletal muscle abnormalities and identifying nutritional interventions capable of maintaining skeletal muscle metabolic and structural homeostasis are important for alleviating metabolic damage associated with nutrient excess [8].

Oxidative stress and inflammation interact closely during the development of HFD-associated skeletal muscle abnormalities [9–11]. Lipid overload increases mitochondrial oxidative burden and ROS production, whereas inflammatory mediators such as TNF-$\alpha$ and IL-6 may further impair mitochondrial function and amplify oxidative stress [10,11]. This reciprocal interaction may also compromise structural homeostasis by affecting cytoskeletal organisation, muscle fibre repair and extracellular matrix (ECM) turnover, partly through regulatory factors such as TGF-$\beta$1. Excessive deposition of collagen and other ECM components can increase tissue stiffness and impair mechanical force transmission and muscle regeneration [11–13]. Thus, inflammation and oxidative stress may link nutrient excess to ECM-related structural alterations in skeletal muscle.

Resveratrol is a naturally occurring polyphenol widely present in food sources such as grapes, berries and peanuts and has attracted considerable attention in functional food and nutritional health research because of its anti-inflammatory, antioxidant and metabolic regulatory properties [14,15]. Recent animal studies have shown that resveratrol can modulate multiple aspects of skeletal muscle homeostasis, including inflammatory, redox, metabolic and mitochondrial responses [16–19]. In a mouse model of sarcopenic obesity, resveratrol attenuated skeletal muscle inflammation and muscle atrophy, suggesting a potential protective effect against obesity-associated muscle injury [16]. In HFD models, resveratrol has been reported to enhance skeletal muscle antioxidant capacity, reduce oxidative stress and improve insulin sensitivity through oxidative stress-related signalling

pathways such as Nrf2–Keap1 [17]. It can also reduce lipid accumulation in skeletal muscle, improve tissue morphology and regulate signalling processes related to glucose uptake, lipid metabolism and protein homeostasis, including the IRS-1/PI3K/AKT/GLUT4 and DDIT4/mTOR pathways [18]. In addition, resveratrol can improve skeletal muscle redox homeostasis and modulate metabolism-related molecular processes [17,18]. In non-human primates exposed to a long-term high-fat/high-sugar diet, resveratrol also attenuated mitochondrial loss and abnormalities in skeletal muscle fibre phenotype [19]. Collectively, these findings indicate that the nutritional protective effects of resveratrol on skeletal muscle may involve redox homeostasis, inflammatory responses, energy metabolism and protein homeostasis [16–19]. Resveratrol may therefore serve as a food-derived bioactive compound for alleviating HFD-induced metabolic and structural abnormalities in skeletal muscle [8].

Although previous studies have demonstrated that resveratrol can influence skeletal muscle metabolism, inflammation and oxidative stress, most investigations have focused on body weight, glucose and lipid metabolism, individual biochemical markers, or classical metabolic and stress-related pathways such as SIRT1/PGC-1$\alpha$, Nrf2–Keap1, IRS-1/PI3K/AKT/GLUT4 and DDIT4/mTOR [8,17,18,20]. Comparatively less attention has been given to the relationship between skeletal muscle morphology and ECM-related transcriptional responses during resveratrol intervention. In particular, it remains unclear whether HFD-associated transcriptional alterations involving collagen and ECM-related processes occur alongside changes in skeletal muscle morphology and inflammatory–oxidative stress status. RNA sequencing provides an opportunity to examine these responses at the transcriptome level and to identify candidate genes showing opposite expression directions between HFD exposure and nutritional intervention.

Accordingly, the present study integrated quadriceps muscle weight measurements, skeletal muscle histomorphology, inflammatory and oxidative stress-related indices, ECM-related biochemical assessments and transcriptomic analysis in HFD-fed rats receiving concurrent resveratrol intervention. Hydroxyproline content and ECM-related protein concentrations were measured to characterise biochemical changes associated with collagen content and matrix regulation. RNA sequencing was used to identify exploratory candidate genes showing opposite expression directions between HFD feeding and resveratrol intervention, with particular attention to collagen- and ECM-related transcriptional processes. Functional enrichment and PPI analyses were used to characterise these candidate transcriptional responses, and selected expression trends were further assessed by RT-qPCR. This integrated approach was designed to characterise ECM-related biochemical and transcriptional responses associated with resveratrol intervention, rather than to establish ECM remodelling as a confirmed causal mechanism.

## 2. Materials and Methods

### *2.1. Experimental Animals and Study Design*

Forty healthy 4-week-old female Sprague–Dawley (SD) rats with comparable initial body weights were obtained from Jiangsu Huachuang Xinnuo Pharmaceutical Technology Co., Ltd. (Jiangsu, China; experimental animal production licence No. SCXK (Su) 2020-0009). The use of female rats was determined by the broader experimental framework: the present skeletal muscle study represented a separate, shorter-duration component of a female-focused research programme examining HFD and resveratrol responses in both reproductive and extra-reproductive tissues. A related longer-term study from our group investigated ovarian responses to HFD and resveratrol in female rats [21]. Previous studies have documented sex-related skeletal muscle responses to obesogenic diets in rodents [22,23], while resveratrol has been shown to modify HFD-associated skeletal muscle

outcomes in female mice [24]. Together, these findings provide experimental context for the use of a female HFD–resveratrol model in the present study.

The animals were kept under specific pathogen-free (SPF) conditions at Anhui Agricultural University with a 12 h light/12 h dark cycle and ad libitum access to food and water. They were allowed to acclimatise for 1 week before group assignment.

After acclimation, animals were randomly distributed among four groups, with 10 rats in each: CON, CONR, HFD and HFDR. Each group occupied two cages, with five animals housed per cage. Standard diet was provided to the CON and CONR groups, whereas the HFD and HFDR groups received a diet in which 45% of total energy was derived from fat. Both diets were custom produced by Jiangsu Synergy Pharmaceutical Bioengineering Co., Ltd. (Jiangsu, China), and their macronutrient composition and energy density are reported in Supplementary Table S5.

Resveratrol (99% purity; Macklin Biochemical Co., Ltd., Shanghai, China) was prepared as a suspension in 2% sodium carboxymethyl cellulose immediately before use and protected from light. Animals assigned to the CONR and HFDR groups were administered resveratrol by oral gavage at 300 mg $kg^{-1}$ body weight $day^{-1}$; the CON and HFD groups received the same volume of the vehicle solution. The selected dose was based on previous rodent studies using relatively high resveratrol exposures. Oral administration of 300 mg $kg^{-1}$ body weight $day^{-1}$ has been reported in rats for metabolic evaluation and safety assessment [25,26], while relatively high resveratrol exposure has also been investigated in HFD rodent models [27]. Thus, the dose used here should be regarded as an experimental rodent exposure rather than a dose intended for direct extrapolation to humans.

The experimental period lasted 5 weeks. HFD exposure and resveratrol administration commenced simultaneously at the start of the intervention. The study therefore represents a concurrent-intervention design rather than a therapeutic model in which resveratrol is introduced after HFD-associated skeletal muscle abnormalities have already been established.

All procedures involving animals were reviewed and approved by the Institutional Animal Care and Use Committee of Anhui Agricultural University (Approval No. AHAU2023–002) and were carried out in accordance with applicable institutional guidelines.

### *2.2. Body Weight, Feed Intake and Sample Collection*

Body weight was recorded once per week after a 12 h fasting period, during which water remained available. Measurements were obtained the following morning with an electronic balance. Each animal was weighed in duplicate, and the average of the two readings was used for analysis.

Feed consumption was monitored on a cage basis. At each feeding interval, both the amount of diet supplied and the uneaten remainder were weighed, and their difference was used to determine feed disappearance. Daily feed intake per animal was estimated by dividing cage-level daily consumption by the number of rats housed in that cage. Daily energy intake was then estimated from feed intake and the energy density of the relevant diet, using 3.83 kcal $g^{-1}$ for the standard diet and 4.70 kcal $g^{-1}$ for the HFD. Because each treatment group comprised two cages, the cage was regarded as the experimental unit for analyses of both feed and estimated energy intake.

At the completion of the 5-week intervention, animals were anaesthetised by intraperitoneal administration of sodium pentobarbital at 40 mg $kg^{-1}$ body weight. Once deep anaesthesia had been confirmed, euthanasia was performed by cervical dislocation and both quadriceps muscles were promptly excised. The wet weight to body weight ratio was calculated as the wet weight of the left quadriceps divided by body weight (mg/g).

The left quadriceps was immersed in GD muscle tissue fixative (Servicebio, Wuhan, China) using a tissue-to-fixative volume ratio of at least 1:10 for histological processing. The contralateral quadriceps was rapidly frozen in liquid nitrogen and kept at −80 °C until biochemical measurements and RNA-seq analysis were performed.

### *2.3. Histological Examination and Muscle Fibre Morphology*

Fixed quadriceps specimens were processed through graded ethanol dehydration, xylene clearing and paraffin embedding. Transverse sections were prepared relative to the orientation of the muscle fibres. After removal of paraffin and rehydration, sections were subjected to haematoxylin and eosin (H&E) staining and subsequently mounted with neutral mounting medium. Microscopic examination and image acquisition were carried out under the same magnification and imaging settings for all samples.

For histological evaluation, nine animals were randomly selected from each experimental group. Three spatially separate, non-overlapping microscopic fields were randomly sampled from each animal. Of these nine animals, three per group were also included in the RNA-seq analysis. Both image acquisition and subsequent ImageJ-based quantification were conducted by investigators who were unaware of the treatment-group identities. Three spatially separate, non-overlapping microscopic fields were randomly sampled from each animal. Both image acquisition and subsequent ImageJ-based quantification were conducted by investigators who were unaware of the treatment-group identities.

Images collected at 100× magnification were quantified with ImageJ (version 1.53k) [28]. Muscle fibre diameter and fibre number were recorded for each field, and fibre density was calculated as the number of fibres per unit tissue area. Field-level measurements were first averaged within each animal, after which the animal-level value was used as the independent observation for statistical analysis.

### *2.4. Determination of Inflammatory and Oxidative Stress-Related Indices in Skeletal Muscle*

Nine animals were randomly chosen from each experimental group for biochemical assessment of quadriceps muscle. These animals were selected from the same ten rats per group, and the biochemical subset therefore overlapped with the animals used for histological examination and RNA-seq analysis. Tissue homogenates were prepared at different concentrations according to the requirements of the individual assays. A 10% homogenate was used for all measurements except total antioxidant capacity (T-AOC), corresponding to a tissue-to-medium ratio of 1:9, whereas T-AOC analysis used a 20% homogenate prepared at a ratio of 1:4. Depending on the assay kit, either 0.9% physiological saline or the specified phosphate-buffered saline (PBS) was used as the homogenisation medium.

Muscle tissue was cut into small pieces on ice and processed with a KZ-II low-temperature tissue grinder (Wanbo Biotechnology Co., Ltd., Shanghai, China) at 65 Hz for two 90 s cycles while maintained at 4 °C. The centrifugation conditions varied according to the subsequent assay. Most homogenates were centrifuged at 2500 r $min^{-1}$ for 10 min at 4 °C, whereas samples intended for $H_2O_2$ and T-AOC measurements were centrifuged at 10,000 r $min^{-1}$ for 10 min and 12,000 r $min^{-1}$ for 5 min, respectively. Supernatants recovered after centrifugation were used for biochemical measurements.

Protein concentration in the homogenates was measured by the Coomassie Brilliant Blue assay. Concentrations of TGF-β1, TNF-α, IL-6 and IL-10 were determined with commercial ELISA kits, while $H_2O_2$, malondialdehyde (MDA), superoxide dismutase (SOD) activity and T-AOC were assessed using their respective biochemical assay kits. All assay kits were obtained from Nanjing Jiancheng Bioengineering Institute (Nanjing, China) and were used in accordance with the supplied protocols.

For the cytokine assays, absorbance was recorded at 450 nm and concentrations were derived from the corresponding standard curves. $H_2O_2$ was quantified by the molybdate colorimetric assay at 405 nm. SOD activity was assessed with the WST-1 method at 450 nm, MDA with the thiobarbituric acid (TBA) method at 532 nm, and T-AOC with the ferric reducing antioxidant power (FRAP) method at 593 nm. Final values were obtained according to the calculation procedures specified for each kit, with protein-normalised indices expressed relative to the protein concentration of the corresponding tissue homogenate.

### *2.5. Determination of ECM-Related Indices in Skeletal Muscle*

Nine animals per group, randomly selected from the same ten rats per group and overlapping with the biochemical subset described in Section 2.4, were used to determine ECM-related indices in quadriceps muscle, including hydroxyproline, LOX, MMP-2, MMP-9, TIMP-1 and TIMP-2.

Hydroxyproline, an indirect indicator of collagen content, was measured using a kit (Nanjing Jiancheng Bioengineering Institute, Nanjing, China). Approximately 50 mg of minced tissue was mixed with 1 mL of alkaline hydrolysis solution and heated in a boiling water bath for 20 min. Hydrolysates were adjusted to pH 6.0–6.8 and diluted according to the kit instructions. An aliquot (2–4 mL) was treated with activated carbon and centrifuged at 3500 rpm for 10 min. Supernatant (1 mL) was used for colour development and absorbance measurement at 550 nm.

For ELISA, tissues were rinsed with ice-cold PBS (0.01 M, pH 7.4), minced and homogenised with nine volumes of PBS using a KZ-II low-temperature tissue grinder (Wanbo Biotechnology, Shanghai, China) at 65 Hz for two 90 s cycles at 4 °C. Homogenates were centrifuged at 5000× *g* for 5 min at 4 °C, and supernatants were diluted as required.

LOX was measured using a FineTest Rat LOX ELISA Kit (Wuhan Fine Biotech Co., Ltd., Wuhan, Hubei, China; ER1769); MMP-2, TIMP-2, MMP-9 and TIMP-1 were measured using CUSABIO Rat ELISA kits (Wuhan Huamei Biotech Co., Ltd., Wuhan, Hubei, China; CSB-E07411r, CSB-E07386r, CSB-E08008r and CSB-E08005r, respectively). Standards or samples (100 μL/well) were incubated for 90 min for LOX/MMP-9 or 2 h for the remaining targets. Wells were washed twice without soaking for LOX; other assays proceeded without washing. Biotin-labelled antibody (100 μL/well) was incubated for 1 h, followed by three washes. HRP conjugate (100 μL/well) was incubated for 30 min for LOX/MMP-9 or 1 h otherwise, followed by five washes. Wash volumes were 350 μL for LOX and 200 μL for CUSABIO assays, with respective soaking periods of 1 and 2 min after antibody/HRP incubation. TMB (90 μL/well) was developed in darkness for 10–20 min for LOX or 15–30 min otherwise. All incubations were at 37 °C. After adding stop solution (50 μL/well), absorbance was read at 450 nm immediately for LOX or within 5 min otherwise. Concentrations were calculated using four-parameter logistic curves and corrected for dilution. MMP-2/TIMP-2 and MMP-9/TIMP-1 ratios were calculated per animal after unit conversion

### *2.6. Total RNA Extraction, Library Construction and Transcriptome Sequencing*

RNA-seq was performed using three biological samples from each experimental group (12 samples in total), selected from the nine animals per group used for histological examination. Total RNA was isolated from quadriceps muscle with TRIzol reagent (Aidlab Biotechnologies Co., Ltd., Beijing, China). RNA quantity and purity were determined using a NanoDrop 2000 spectrophotometer (Thermo Fisher Scientific, Waltham, MA, USA), while RNA integrity was examined by agarose gel electrophoresis and further assessed using an Agilent 2100 Bioanalyzer (Agilent Technologies, Santa Clara, CA, USA).

Only RNA samples that satisfied the required quality criteria were used for library preparation. Polyadenylated RNA was captured with oligo(dT) magnetic beads and subsequently fragmented. First-strand cDNA was synthesised from the fragmented RNA using random oligonucleotide primers, followed by synthesis of the complementary strand. The resulting double-stranded cDNA fragments were processed through end repair, A-tail addition, adaptor ligation and size selection before PCR enrichment. Library concentration was first measured using a Qubit 2.0 fluorometer, and fragment-size distribution was examined with an Agilent 2100 Bioanalyzer. Following qPCR-based determination of effective library concentration, qualified libraries were sequenced on an Illumina platform in paired-end mode, producing 150 bp reads from both ends.

### *2.7. RNA-Seq Data Processing and Differential Expression Analysis*

Raw sequence data were filtered before downstream analysis. Reads containing adaptor contamination, an excessive proportion of undetermined bases, or low-quality sequence were excluded. Quality characteristics of the retained reads were summarised using Q20, Q30 and GC content. The rat reference genome assembly and gene annotation corresponding to accession GCF_036323735.1 were obtained from the National Center for Biotechnology Information (NCBI). A reference index was generated with HISAT2 (version 2.0.5) [29], which was subsequently used to map the filtered paired-end reads to the rat genome.

Gene-level counts were generated with featureCounts (version 2.1.1) [30]. FPKM values were calculated separately for visualisation purposes, including gene-expression distributions, heatmaps and related expression plots. Differential-expression testing was conducted in DESeq2 (version 1.20.0) [31] using the raw gene-count matrix.

An initial exploratory screen defined candidate differentially expressed genes (DEGs) as those with a nominal $p < 0.05$ and $|\log_2(\text{fold change})| > 0.585$, equivalent to a change greater than 1.5-fold. Volcano plots were produced in R (version 3.6.3), and the numbers of upregulated and downregulated candidates were summarised for each comparison.

Candidate genes showing opposite expression responses to HFD feeding and resveratrol intervention were then identified by comparing the HFD versus CON and HFDR versus HFD contrasts. Genes increased in HFD versus CON and decreased in HFDR versus HFD were combined with genes showing the reciprocal pattern. The resulting 112 genes were designated as directionally reversed candidate genes. Here, "directionally reversed" refers only to opposite $\log_2$ fold-change directions between the two comparisons and does not imply restoration to control expression levels.

To evaluate the robustness of the exploratory screening to multiple testing, Benjamini–Hochberg-adjusted $p$ values were examined while retaining the same $|\log_2(\text{fold change})|$ threshold. Genes satisfying FDR < 0.05 together with $|\log_2(\text{fold change})| > 0.585$ were classified as FDR-supported DEGs. The original 112 directionally reversed genes were retained as an exploratory candidate set, whereas genes satisfying the FDR and fold-change criteria in both the HFD versus CON and HFDR versus HFD comparisons while maintaining opposite expression directions were classified as the strict FDR-supported reversed subset.

https://doi.org/10.3390/cells15232177

Expression of the 112 exploratory candidates was additionally examined in the HFDR versus CON comparison to determine whether their expression approached the control condition. Benjamini–Hochberg-adjusted *p* values were used to assess whether individual genes remained significantly different from CON. Lack of statistical significance in this comparison was not considered evidence of equivalence, normalisation or complete restoration.

Expression recovery was also characterised descriptively using a recovery fraction calculated for each candidate gene as 1 − |HFDR mean − CON mean|/|HFD mean − CON mean| from median-ratio-normalised count data. Values closer to 1 represent a smaller residual difference from the CON mean after resveratrol intervention, whereas values below 0 indicate a larger deviation from CON than that observed in the HFD group. This metric was used only for descriptive assessment and was not interpreted as inferential evidence of expression normalisation.

### *2.8. Functional Enrichment and Protein–Protein Interaction Network Analyses*

The 112 directionally reversed candidate genes were subjected to exploratory Gene Ontology (GO) and Kyoto Encyclopedia of Genes and Genomes (KEGG) over-representation analyses. Genes represented in the expression dataset and carrying the corresponding GO or KEGG annotations served as the reference background. Functional enrichment analysis was conducted using clusterProfiler (version 3.8.1) [32]. GO terms were evaluated separately within the Biological Process (BP), Cellular Component (CC) and Molecular Function (MF) domains. Enrichment significance was assessed with a one-sided hypergeometric test, followed by Benjamini–Hochberg correction for multiple comparisons; terms with FDR < 0.05 were considered statistically significant. Because only five genes satisfied the strict FDR-supported reversed criteria, this subset was not subjected to formal pathway-enrichment testing owing to its limited size. Accordingly, enrichment based on the 112-gene set was regarded as exploratory and hypothesis-generating. Enrichment patterns were displayed using GeneRatio, enriched-gene counts and $-\log_{10}$(FDR).

Protein–protein interaction relationships among the 112 exploratory candidates were retrieved from the STRING database (version 12.0) [33] for Rattus norvegicus. A minimum combined interaction score of 0.150 was used for the primary analysis. Interaction records associated with the HFD versus CON and HFDR versus HFD comparisons were merged, after which edges were retained only when both interacting nodes belonged to the 112-gene candidate set. For duplicated undirected node pairs, only the interaction with the larger combined score was retained.

The resulting interactions were represented as an undirected weighted network using NetworkX (version 3.6.1) in Python (version 3.15.2), with graphical output generated in Matplotlib (version 3.10.8). Connectivity of individual genes was summarised by node degree, defined here as the number of unique interaction edges linked to that node. Network layout was generated using a force-directed algorithm; node size reflected degree, whereas edge width represented the STRING combined score. Because the network was derived from the exploratory 112-gene set, connectivity measures were interpreted descriptively and were not considered confirmatory evidence of FDR-supported differential expression.

To examine the dependence of network structure on the STRING confidence cutoff, an additional sensitivity analysis was performed using a higher combined-score threshold of 0.400; the resulting network characteristics are summarised in Supplementary Table S4. Finally, candidate genes related to extracellular matrix organisation and collagen-associated processes were selected on the basis of the exploratory enrichment results and functional annotations to generate an ECM-related PPI subnetwork.

### *2.9. RT-qPCR*

For RT-qPCR analysis, three rats per group were selected from the same experimental cohort; these animals did not overlap with the rats used for RNA-seq and histological analyses. Total RNA was isolated with TRIzol reagent. Genomic DNA was removed and cDNA was synthesised using the TRUEscript RT MasterMix with OneStep gDNA Removal kit (Aidlab Biotechnologies Co., Ltd., Beijing, China). Reverse transcription was carried out in a final volume of 20 μL at 42 °C for 15 min, followed by 85 °C for 5 s.

Quantitative PCR was performed on a CFX96 Touch Real-Time PCR Detection System (Bio-Rad, Hercules, CA, USA) using 2× SYBR Green qPCR Mix (Universal ROX; Aidlab Biotechnologies Co., Ltd., Beijing, China), with methodological reporting guided by the MIQE recommendations [34]. Each 20 μL reaction comprised 10 μL of 2× SYBR Green qPCR Mix, 1 μL of cDNA, 0.4 μL of each primer and nuclease-free water. Thermal cycling began with 120 s at 95 °C and was followed by 40 cycles of 95 °C for 15 s and 60 °C for 33 s. A melting-curve analysis was subsequently performed to verify amplification specificity.

Four genes, Fbn1, Postn, Myoc and Col6a2, were chosen from the exploratory ECM-related candidate set. Actc1 was included separately as a representative muscle structural/contractile-related gene because ACTC1 encodes a striated-muscle $\alpha$-actin isoform that is expressed in skeletal muscle and can contribute to actomyosin-based contractile function [35,36]. These five genes were examined to assess selected expression patterns identified by RNA-seq. Oligonucleotide primers were synthesised by Sangon Biotech Co., Ltd. (Shanghai, China), and their sequences are listed in Supplementary Table S1. Each biological sample was analysed in three technical replicates, from which the average Ct value was used for subsequent calculations. GAPDH served as the reference gene because its Ct values were stable among the CON, CONR, HFD and HFDR groups under the present experimental conditions. Relative transcript abundance was calculated using the $2^{-\Delta\Delta Ct}$ method [37].

For comparison with the RNA-seq results, RT-qPCR expression values were converted to $\log_2$ fold changes for the corresponding group contrasts. Exploratory simple linear regression was then applied to the RNA-seq- and RT-qPCR-derived $\log_2$ fold-change values. Each regression contained one data point for each of the five selected genes.

### *2.10. Statistical Analysis*

GraphPad Prism (version 8.0) was used for statistical testing and preparation of quantitative graphs, while R software (version 3.6.3) was used for RNA-seq-associated analyses and visualisation. Unless otherwise specified, quantitative data are reported as mean ± standard error of the mean (SEM). For animal-level outcomes, the individual animal served as the independent experimental unit; technical replicates and multiple microscopic fields obtained from the same animal were not treated as independent observations.

Changes in body weight across the 5-week intervention were evaluated by two-way repeated-measures ANOVA, with treatment group considered the between-subject factor and time the within-subject factor. Tukey's multiple-comparison procedure was subsequently applied for comparisons among groups. Total body weight gain, quadriceps wet weight, quadriceps wet weight-to-body weight ratio, histomorphological measurements, inflammatory and oxidative stress-related indices, and ECM-related biochemical indices were evaluated using two-way ANOVA, with diet (standard diet or HFD) and resveratrol administration (vehicle or resveratrol) entered as fixed factors. Diet effects, resveratrol effects and their interaction were examined, followed, where appropriate, by Tukey-adjusted post hoc comparisons.

Feed intake and estimated energy intake were analysed at the cage level because feed consumption was recorded collectively for each cage. With only two cages available in each experimental group, these measurements were treated primarily as descriptive data and were not used to infer individual-animal differences or to artificially increase the effective sample size. Statistical significance was defined as $p < 0.05$.

The relationship between RNA-seq- and RT-qPCR-derived $\log_2$ fold changes was explored using simple linear regression. Because only five selected genes contributed to each regression, this analysis was considered exploratory and was used to examine agreement in expression-change patterns rather than to establish quantitative equivalence between the two methods.

## 3. Results

### *3.1. Effects of Resveratrol on Body Weight Gain, Feed Intake and Relative Quadriceps Mass*

The experimental design is shown in Figure 1A. Rats received either a standard diet or an HFD and were administered vehicle or resveratrol by oral gavage for 5 weeks. Body weight increased progressively in all groups throughout the intervention period (Figure 1C). In terms of the overall body weight trajectory, rats in the HFD group showed higher body weights than those in the CON group during the later stages of the intervention, whereas body weights in the CONR and HFDR groups tended to be lower than those in their respective untreated groups (Figure 1C). Analysis of total body weight gain showed a downward trend in the CONR group compared with the CON group and in the HFDR group compared with the HFD group; however, neither comparison reached statistical significance ($p > 0.05$; Figure 1B). Two-way ANOVA showed significant main effects of diet ($p = 0.0015$) and resveratrol ($p = 0.0073$) on total body weight gain, with no significant Diet × Resveratrol interaction ($p = 0.6630$; Supplementary Table S6). Both the wet weight of the left quadriceps and its wet weight-to-body weight ratio were significantly lower in the HFD group than in the CON group and significantly higher in the HFDR group than in the HFD group ($P < 0.01$; Supplementary Figure S1A,B). Average daily feed intake, recorded at the cage level, generally increased over the intervention period (Figure 1D). Descriptively, feed intake by mass was generally higher in the CON and CONR groups, whereas the HFD-fed groups consumed less feed by mass. When feed intake was converted to estimated energy intake using the corresponding diet energy densities, the HFD group generally showed higher energy intake than the standard-diet groups despite its lower feed intake by mass, whereas the HFDR group showed lower estimated energy intake than the HFD group during the intervention period (Figure 1E). Because feed intake and estimated energy intake were derived from only two cages per group, these data were interpreted descriptively and were not subjected to individual-level statistical inference.

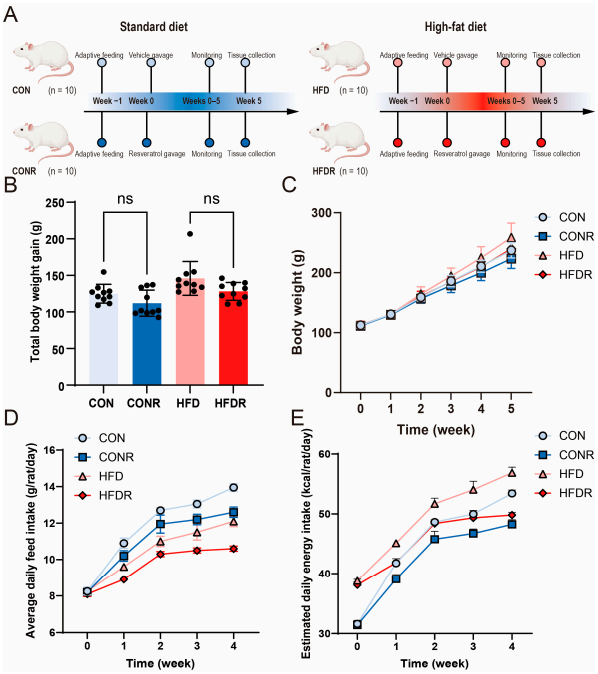


https://doi.org/10.3390/cells15232177

**Figure 1.** Effects of resveratrol supplementation on body weight gain and feed intake in rats fed a standard or high-fat diet. (**A**) Experimental design. Rats were acclimated for 1 week and randomly assigned to four groups: CON, CONR, HFD, and HFDR. Vehicle or resveratrol (300 mg $kg^{-1}$ body weight $day^{-1}$) was administered by oral gavage for 5 weeks. HFD feeding and resveratrol administration were initiated concurrently at the beginning of the 5-week intervention period. (**B**) Total body weight gain, analysed using two-way ANOVA with diet and resveratrol treatment as fixed factors, followed by Tukey's multiple-comparison test. (**C**) Weekly body weight changes, analysed using two-way repeated-measures ANOVA followed by Tukey's multiple-comparison test. (**D**) Average daily feed intake measured at the cage level and presented descriptively because only two cages were available per group. Body weight data were obtained from individual rats (n = 10 per group), whereas feed intake was calculated from two cages per group. Data are presented as mean ± SEM. ns, not significant. (**E**) Estimated daily energy intake, calculated from average daily feed intake and the energy density of the corresponding diet (3.83 kcal $g^{-1}$ for the standard diet and 4.70 kcal $g^{-1}$ for the HFD). Feed and energy intake data were obtained at the cage level and are presented descriptively because only two cages were available per group.

### *3.2. Effects of Resveratrol on Skeletal Muscle Morphology*

H&E staining showed clearly defined transverse muscle fibre structures in the quadriceps of all groups (Figure 2A–D). Compared with the corresponding groups without resveratrol supplementation under the same dietary condition, the resveratrol-treated groups showed differences in muscle fibre arrangement and reduced inter-fibre spaces (Figure 2A–D). Two-way ANOVA followed by Tukey's multiple-comparison test showed that average muscle fibre diameter was significantly higher in the HFD group than in the CON group and significantly lower in the HFDR group than in the HFD group ($p < 0.01$; Figure 2E). In parallel, muscle fibre density was significantly lower in the HFD group than in the CON group and significantly higher in the HFDR group than in the HFD group ($p < 0.01$; Figure 2F). These findings indicate that resveratrol supplementation was associated with alterations in quadriceps muscle fibre morphology, characterised primarily by increased fibre density and decreased average fibre diameter. Two-way ANOVA showed significant main effects of diet and resveratrol treatment on both muscle fibre density and diameter (all $p < 0.05$), with no significant Diet × Resveratrol interactions (Supplementary Table S6).

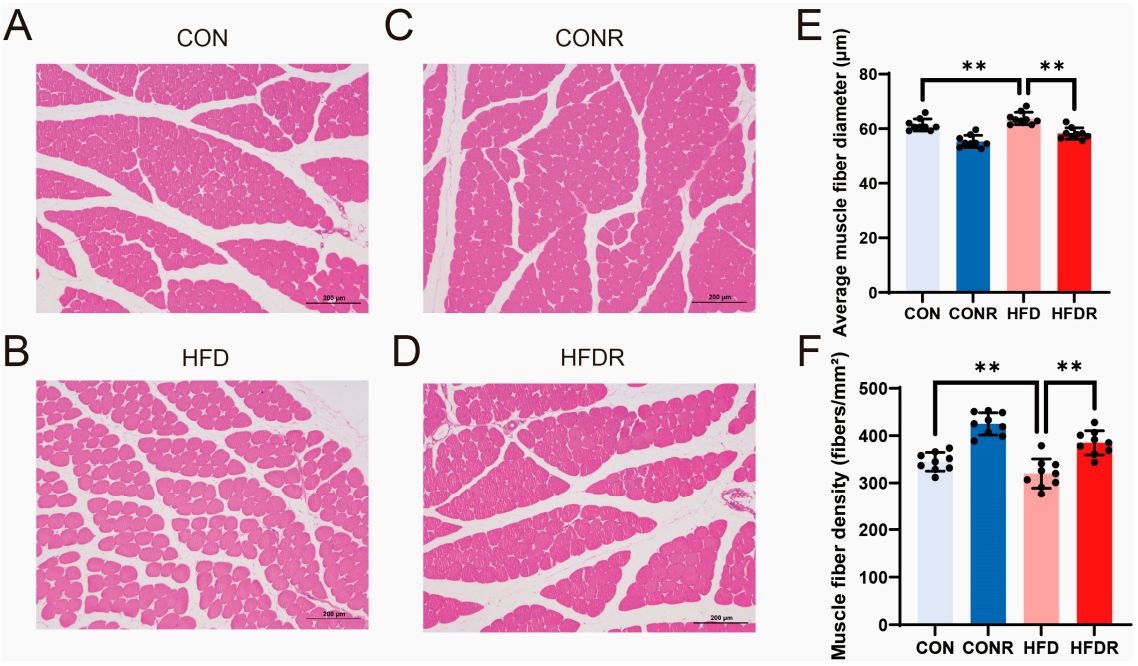

**Figure 2.** Effects of resveratrol supplementation on quadriceps muscle histomorphology in rats fed a standard or high-fat diet. Representative H&E-stained sections of quadriceps muscle from (**A**) CON, (**B**) HFD, (**C**) CONR, and (**D**) HFDR groups. (**E**) Average muscle fibre diameter and (**F**) muscle fibre density. Multiple microscopic fields were averaged for each animal before statistical analysis, and each dot represents one biological replicate (n = 3 per group). Data are presented as mean ± SEM and were analysed using two-way ANOVA with diet and resveratrol treatment as fixed factors, followed by Tukey's multiple-comparison test. ** $p < 0.01$. Scale bars, 200 μm.

### *3.3. Effects of Resveratrol on Inflammatory and Oxidative Stress-Related Indices in Skeletal Muscle*

Compared with the CON group, the HFD group showed significantly higher quadriceps muscle levels of TGF-β1, TNF-α, IL-6, $H_2O_2$ and MDA, together with significantly lower IL-10 levels, SOD activity and T-AOC ($p < 0.01$; Figure 3A–H). Compared with the HFD group, the HFDR group showed significantly lower TGF-β1, $H_2O_2$ and MDA levels and significantly higher IL-10 and T-AOC levels ($p < 0.01$; Figure 3A,D–F,H). In contrast, TNF-α, IL-6 and SOD activity did not differ significantly between the HFDR and HFD groups ($p > 0.05$; Figure 3B,C,G). These results indicate that, under the present experimental conditions, concurrent resveratrol intervention was associated with selective differences in inflammatory and oxidative stress-related indices during HFD feeding. Significant main effects of diet and resveratrol were detected for all eight indices (all $p < 0.05$), whereas significant Diet × Resveratrol interactions were observed only for MDA and T-AOC (Supplementary Table S6).

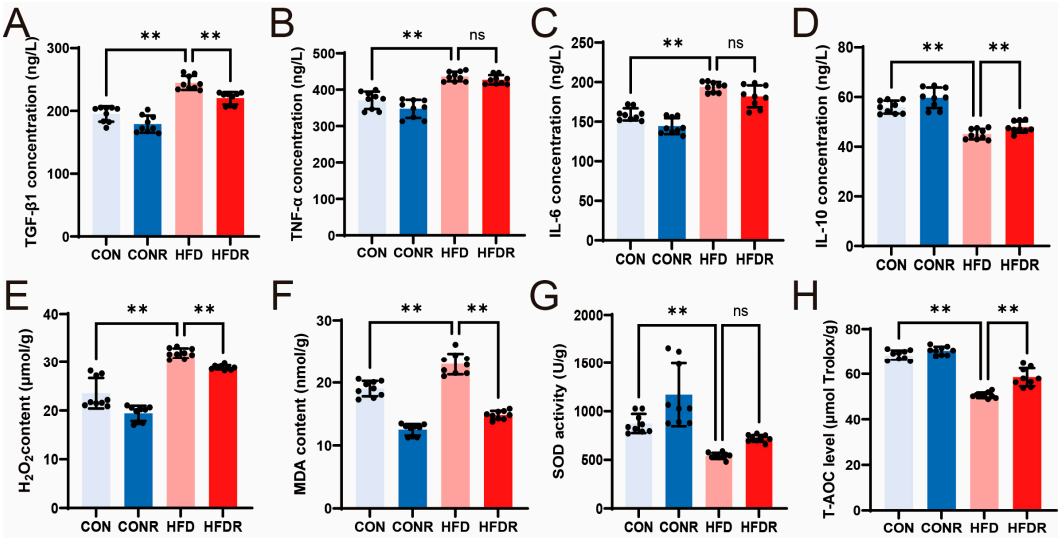


**Figure 3.** Effects of resveratrol supplementation on inflammatory and oxidative stress-related indices in quadriceps muscle of rats fed a standard or high-fat diet. Quadriceps muscle levels of (**A**) TGF-β1, (**B**) TNF-α, (**C**) IL-6, (**D**) IL-10, (**E**) $H_2O_2$, (**F**) MDA, (**G**) SOD activity, and (**H**) T-AOC in the CON, CONR, HFD, and HFDR groups. Data are presented as mean ± SEM, and each dot represents one biological replicate (n = 9 per group). Statistical differences were analysed using two-way ANOVA with diet and resveratrol treatment as fixed factors, followed by Tukey's multiple-comparison test. ** $p < 0.01$; ns, not significant.

### *3.4. Effects of Resveratrol on ECM-Related Biochemical Indices in Skeletal Muscle*

To further characterise ECM-related biochemical responses, hydroxyproline content and the concentrations of LOX, MMP-2, MMP-9, TIMP-1 and TIMP-2 were measured in quadriceps muscle. Compared with the CON group, the HFD group showed significantly higher hydroxyproline, LOX, MMP-2 and MMP-9 levels, significantly lower TIMP-1 and

TIMP-2 levels, and higher MMP-2/TIMP-2 and MMP-9/TIMP-1 ratios ($p < 0.01$; Figure 4A–H). Compared with the HFD group, the HFDR group showed significantly lower hydroxyproline, LOX, MMP-2 and MMP-9 levels, significantly higher TIMP-1 and TIMP-2 levels, and lower MMP-2/TIMP-2 and MMP-9/TIMP-1 ratios ($p < 0.01$; Figure 4A–H). These findings indicate that concurrent resveratrol intervention attenuated HFD-associated changes in collagen-related biochemical content and ECM regulatory protein concentrations.

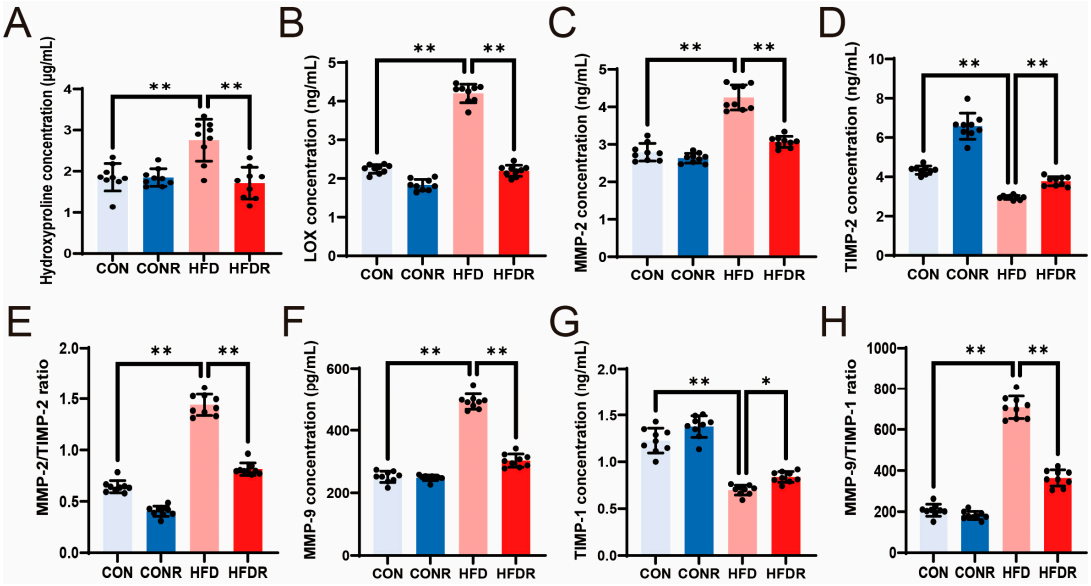


**Figure 4.** Effects of resveratrol supplementation on ECM-related biochemical indices in quadriceps muscle of rats fed a standard or high-fat diet. (**A**) Hydroxyproline content measured using a colorimetric assay. Concentrations of (**B**) LOX, (**C**) MMP-2, (**D**) TIMP-2, (**F**) MMP-9 and (**G**) TIMP-1 were measured by ELISA. The (**E**) MMP-2/TIMP-2 and (**H**) MMP-9/TIMP-1 concentration ratios were calculated for each animal. Data are presented as mean ± SEM, and each dot represents one biological replicate (n = 9 per group). Statistical differences were analysed using two-way ANOVA with diet and resveratrol treatment as fixed factors, followed by Tukey's multiple-comparison test. ** $p < 0.01$; ns, not significant.

### *3.5. Effects of Resveratrol on the Skeletal Muscle Transcriptomic Profile*

RNA-seq quality assessment showed that clean-read numbers, clean-read retention rates and reference-genome mapping efficiencies were comparable across samples, while gene-expression distributions were also generally similar, indicating good overall data quality and comparability (Supplementary Figure S2A–D). Pearson correlation analysis showed high correlations among overall sample expression profiles ($r > 0.95$; Supplementary Figure S3B). Principal component analysis (PCA) showed that the treatment groups were not completely separated and that some within-group dispersion was present (Supplementary Figure S3A).

Using the exploratory screening criteria of $p < 0.05$ and $|\log_2(\text{fold change})| > \log_2(1.5)$, 628 candidate DEGs were identified in the HFD versus CON comparison, including 217 upregulated and 411 downregulated genes. The HFDR versus HFD comparison yielded 589 candidate DEGs, comprising 128 upregulated and 461 downregulated genes. In the CONR versus CON comparison, 477 candidate DEGs were identified, including 124 upregulated and 353 downregulated genes (Figure 5A–D).

An FDR-based re-evaluation was subsequently performed using Benjamini–Hochberg-adjusted $p$ values together with the same $|\log_2(\text{fold change})| > 0.585$ threshold. This analysis identified 35, 67 and 10 FDR-supported DEGs in the HFD versus CON, HFDR versus HFD and CONR versus CON comparisons, respectively.

The HFD versus CON and HFDR versus HFD comparisons were further integrated to identify candidate genes showing opposite expression directions between the two comparisons. A total of 112 candidate genes showed opposite expression directions, including 85 with an HFD-upregulated/HFDR-downregulated pattern and 27 with an HFD-downregulated/HFDR-upregulated pattern (Figure 5E,F).

Among these 112 exploratory candidates, 15 met FDR < 0.05 in the HFD versus CON comparison and 25 met FDR < 0.05 in the HFDR versus HFD comparison. Only five genes—Pi16, Dpt, Loxl1, Slc25a25 and Mfap5—met the FDR < 0.05 and $|\log_2(\text{fold change})| > 0.585$ criteria in both comparisons while retaining opposite expression directions. Therefore, the 112-gene set was retained as an exploratory and hypothesis-generating candidate set rather than being interpreted as a set of FDR-confirmed differentially expressed genes.

To determine whether these opposite-direction changes were accompanied by expression levels approaching those of the CON group, an additional HFDR versus CON comparison was performed, which identified 94 FDR-supported DEGs using the same FDR and fold-change criteria. Among the 112 exploratory candidates, 107 did not differ significantly between HFDR and CON at FDR < 0.05, whereas two remained significantly higher and three remained significantly lower in HFDR than in CON. Importantly, the absence of a significant difference was not interpreted as evidence of equivalence or complete restoration.

Descriptive analysis using median-ratio-normalised expression values showed that 107 of the 112 candidates had a smaller absolute deviation from the CON mean in HFDR than in HFD, whereas five showed a greater deviation. The median recovery fraction was 0.868 (range, −2.736 to 0.995). These findings indicate that many candidate genes showed expression changes in the direction of the control group, but they do not establish normalisation or restoration of expression.

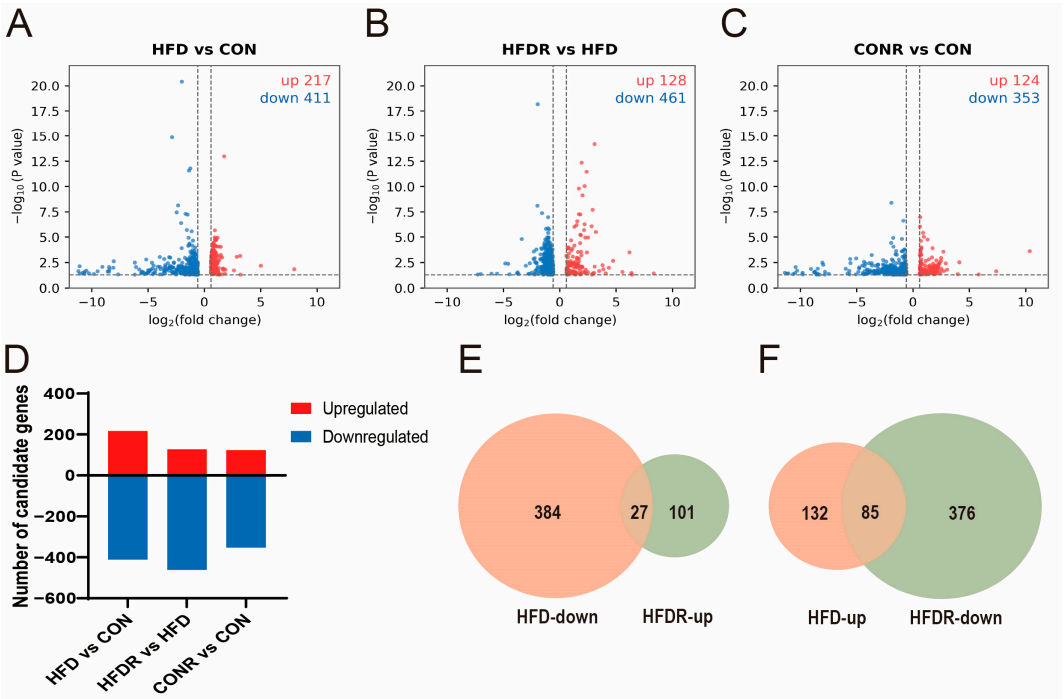


**Figure 5.** Transcriptomic profiling identifies candidate differentially expressed genes and directionally reversed resveratrol-responsive genes in quadriceps muscle. (**A**–**C**) Volcano plots showing candidate differentially expressed genes in HFD vs. CON, HFDR vs. HFD, and CONR vs. CON comparisons. Red and blue dots indicate upregulated and downregulated genes, respectively. The numbers of upregulated and downregulated genes are indicated in each panel based on the criteria of *p*

< 0.05 and $|\log_2(\text{fold change})| > \log_2(1.5)$. (**D**) Summary of candidate differentially expressed genes among the three comparisons. (**E**,**F**) Venn diagrams showing genes with opposite expression directions between HFD-induced changes and resveratrol-associated changes. A total of 112 candidate genes showed opposite expression patterns after resveratrol intervention, including 27 genes downregulated by HFD and upregulated by resveratrol, and 85 genes upregulated by HFD and downregulated by resveratrol. Directional reversal refers only to opposite $\log_2$ fold-change directions in the HFD versus CON and HFDR versus HFD comparisons and does not imply restoration or normalisation of expression to the CON level.

### *3.6. ECM-Related Transcriptional Network Features Associated with Directionally Reversed Candidate Genes*

Hierarchical clustering of the 112 directionally reversed candidate genes showed two opposite expression patterns, comprising 85 genes that were upregulated by HFD and downregulated in HFDR and 27 genes that were downregulated by HFD and upregulated in HFDR (Figure 6A). Among these, the ECM-related genes Myoc, Col6a2, Fbn1 and Postn displayed notable directional changes, indicating that resveratrol intervention was associated with altered HFD-related ECM-associated transcriptional responses. After Benjamini–Hochberg correction, GO analysis identified collagen fibril organisation and extracellular matrix organisation as significantly enriched biological process terms (Figure 6B; Figure S4A). The complete GO enrichment results across biological process, cellular component and molecular function categories are presented in Figure S4A–C. In the KEGG analysis, protein digestion and absorption was the only pathway that remained significantly enriched at FDR < 0.05, whereas ECM–receptor interaction did not meet the FDR significance threshold.

The PPI network constructed using STRING version 12.0 contained 76 directionally reversed candidate genes and 313 non-redundant interaction edges (Figure 6D; Supplementary Figure S5A). Multiple interconnected groups of genes were evident within the network, with relatively dense interactions among ECM-related genes. An ECM-related PPI subnetwork further showed extensive interactions among Col3a1, Fbn1, Postn, Col6a1, Col6a2, Col5a2, Timp1 and Pcolce (Supplementary Figure S5C). Ranking by node degree identified Col3a1 (degree = 34) as the most highly connected node, followed by Fbn1 (27), Col5a2 (25), Timp1 (22), Col6a1 (21), Postn (21), Pcolce (21), Loxl1 (19), Ccdc80 (19) and Pdgfrl (19) (Supplementary Figure S5B). Sensitivity analysis using a more stringent STRING combined-score threshold of ≥0.400 reduced the network from 76 connected nodes and 313 non-redundant edges to 41 connected nodes and 62 edges. Col3a1 and Fbn1 retained the first and second degree ranks, respectively, while Col5a2, Col6a1 and Postn remained among the relatively highly connected nodes. However, the degree-based rankings of several other nodes changed, and Pdgfrl had no retained interactions at the stricter threshold. Thus, relatively high connectivity of several ECM-related nodes persisted, whereas overall network connectivity and the ranking of some individual nodes were sensitive to the STRING confidence threshold (Supplementary Table S4). These highly connected genes showed opposite $\log_2$ fold-change directions in the HFD versus CON and HFDR versus HFD comparisons, indicating distinct HFD-associated and resveratrol-associated expression patterns (Supplementary Figure S5D).

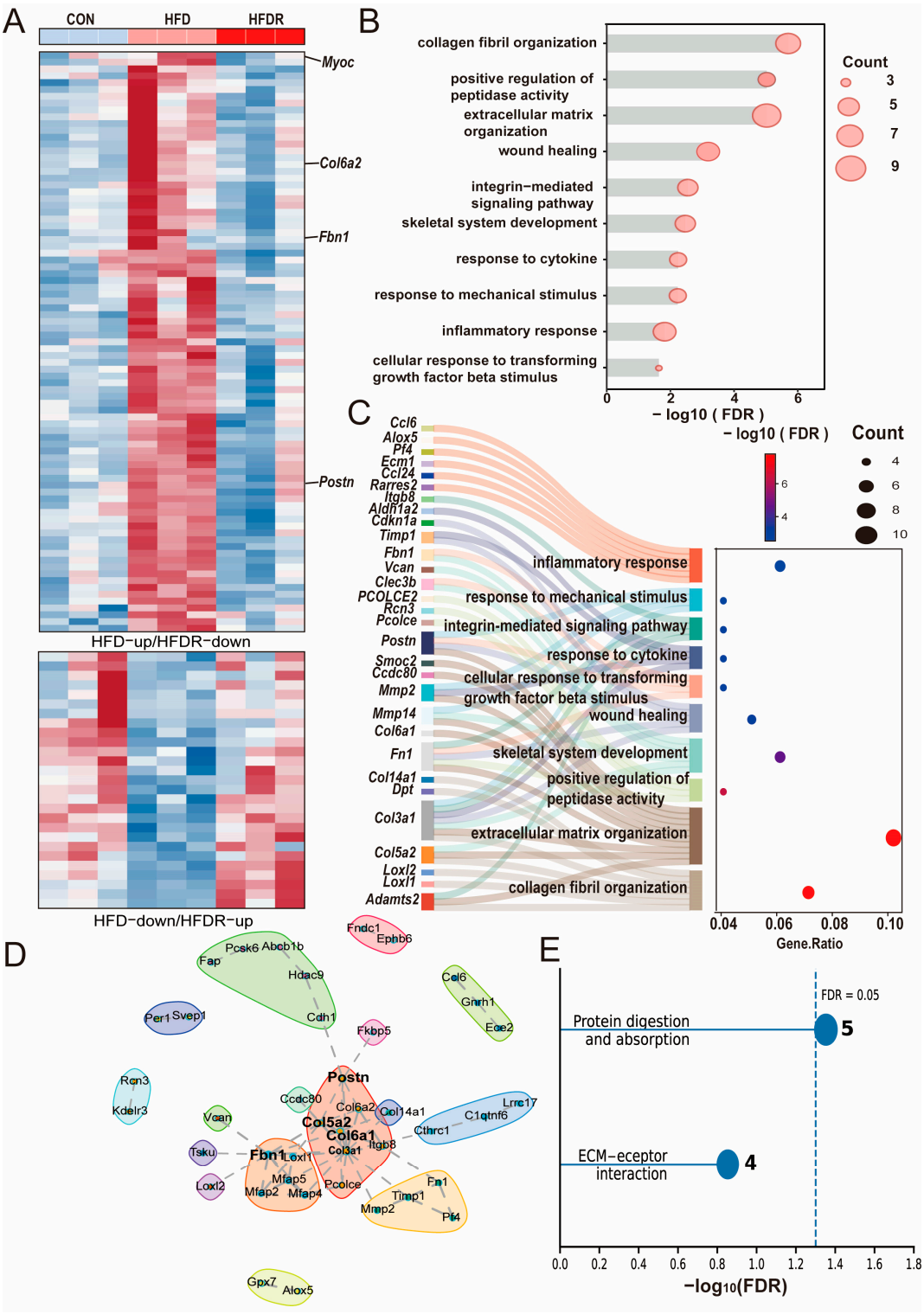


**Figure 6.** Functional enrichment and protein–protein interaction network analysis of directionally reversed candidate genes. (**A**) Heatmaps showing the expression patterns of the 112 directionally reversed genes across the CON, HFD and HFDR groups. The upper heatmap contains 85 genes upregulated in HFD versus CON and downregulated in HFDR versus HFD, whereas the lower heatmap contains 27 genes downregulated in HFD versus CON and upregulated in HFDR versus HFD. Red and blue indicate relatively higher and lower expression levels, respectively; each group comprised three biological replicates. (**B**) Representative enriched Gene Ontology (GO) biological processes associated with the directionally reversed genes. The horizontal axis represents $-\log_{10}$(FDR), and bubble size represents the number of enriched genes. (**C**) Relationships between

representative directionally reversed genes and enriched GO biological processes. The alluvial diagram links representative genes to their associated biological processes, whereas the bubble plot summarises enrichment according to GeneRatio, gene count and $-\log_{10}$(FDR). (**D**) Protein–protein interaction (PPI) network of directionally reversed genes constructed using STRING version 12.0. Node size reflects node degree, and edge width represents the STRING combined score. (**E**) KEGG pathway enrichment analysis of the exploratory 112-gene candidate set after Benjamini–Hochberg correction. The horizontal axis represents $-\log_{10}$(FDR), and the vertical dashed line indicates the FDR = 0.05 threshold [$-\log_{10}(0.05) = 1.301$]. Protein digestion and absorption remained significantly enriched (FDR = 0.0444), whereas ECM–receptor interaction did not meet the FDR significance threshold (FDR = 0.1402). Numbers adjacent to the points indicate the numbers of genes associated with each pathway.

### *3.7. RT-qPCR Assessment of Selected RNA-Seq Expression Trends*

To assess selected RNA-seq expression trends, five representative genes (Fbn1, Postn, Myoc, Actc1 and Col6a2) were examined by RT-qPCR using three rats per group from the same experimental cohort, with no overlap with the rats used for RNA-seq and histological analyses. In the HFD versus CON comparison, Fbn1, Postn, Myoc and Col6a2 were upregulated, whereas Actc1 was downregulated by RT-qPCR, with the direction of change for each gene matching that observed by RNA-seq (Figure 7A). Exploratory cross-gene regression between RNA-seq- and RT-qPCR-derived $\log_2$ fold changes did not reach statistical significance ($R^2 = 0.396$, $p = 0.255$; Supplementary Figure S6A).

In the HFDR versus HFD comparison, Fbn1, Postn, Myoc, Actc1 and Col6a2 were all downregulated by RT-qPCR, again matching the direction of change observed by RNA-seq (Figure 6B). Importantly, because Actc1 was downregulated in both the HFD versus CON and HFDR versus HFD comparisons, it did not show a directionally reversed expression pattern and was not classified as a directionally reversed candidate gene. The corresponding exploratory cross-gene regression was also not statistically significant ($R^2 = 0.628$, $p = 0.110$; Supplementary Figure S6B). Given the small number of selected genes included in each regression (n = 5), these regression analyses were interpreted as exploratory assessments of quantitative concordance rather than as statistical validation of RNA-seq results.

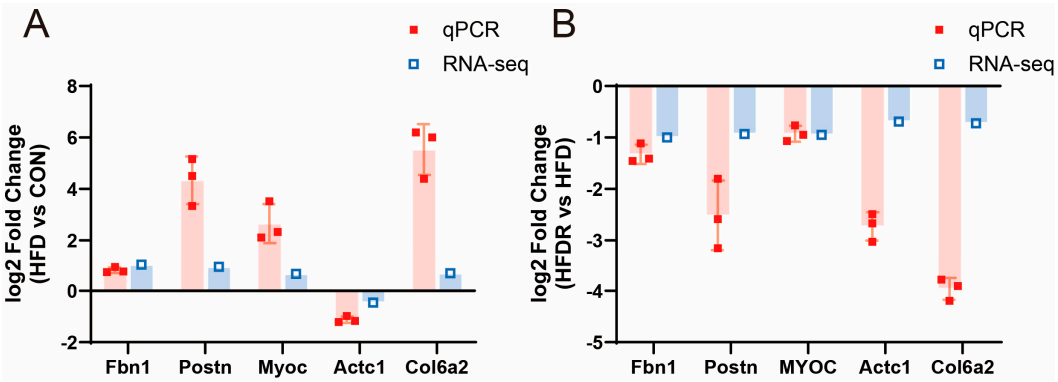


**Figure 7.** RT-qPCR assessment of representative RNA-seq-derived gene expression trends in the quadriceps muscle of rats fed a high-fat diet and treated with resveratrol. (**A**) Comparison of the $\log_2$ fold changes of representative genes (Fbn1, Postn, Myoc, Actc1 and Col6a2) determined by RT-qPCR and RNA-seq in the HFD versus CON comparison. (**B**) Comparison of the $\log_2$ fold changes of the same representative genes determined by RT-qPCR and RNA-seq in the HFDR versus HFD comparison. RT-qPCR data are presented as mean ± SEM from three biological replicates per group selected from the same experimental cohort, with no overlap with the rats used for RNA-seq and histological analyses; three technical replicates were performed for each biological sample. RNA-seq values represent $\log_2$ fold changes obtained from differential-expression analysis. Actc1 was

included as a representative muscle structural/contractile-related gene and was not classified as a directionally reversed candidate gene.

## 4. Discussion

The present study showed that concurrent resveratrol intervention was associated with changes in skeletal muscle morphology during short-term high-fat diet (HFD) feeding in rats. These morphological changes included a more compact muscle fibre arrangement, reduced inter-fibre spaces, increased muscle fibre density and decreased average muscle fibre diameter. Although pairwise comparisons of total body weight gain between resveratrol-treated and corresponding untreated groups were not statistically significant, two-way ANOVA revealed a significant main effect of resveratrol. Therefore, the observed skeletal muscle responses cannot be assumed to be independent of body weight changes, and their functional significance cannot be determined from the present morphological measurements alone. Previous studies have reported effects of resveratrol on skeletal muscle mitochondrial, metabolic and inflammatory pathways under metabolic stress [16,20,38–40], although these mechanisms were not directly assessed here. Differences in dose, duration and experimental model may contribute to variability in body weight responses to resveratrol intervention. Because the HFD had a higher energy density than the standard diet, feed intake by mass alone did not fully reflect dietary energy exposure. We therefore additionally estimated energy intake using the diet-specific energy densities. However, because both feed intake and estimated energy intake were derived from only two cages per group, these data were interpreted descriptively and should not be used for strong individual-level inference. Future studies with additional cage-level replication or pair-feeding designs are needed to clarify the relationship between energy intake and body weight responses. HFD feeding can disrupt skeletal muscle structural homeostasis through lipid accumulation, chronic low-grade inflammation and oxidative stress, and the magnitude of these effects may be influenced by sex, muscle fibre type and intervention duration [11,22–24]. In the present study, the decrease in mean muscle fibre diameter alone cannot be interpreted as evidence of beneficial structural or functional change. The accompanying increase in fibre density per unit area may partly reflect the smaller average fibre size, rather than an independent improvement in muscle quality. Although the resveratrol-treated groups showed a more compact histological appearance and reduced inter-fibre spaces, these observations should be interpreted as morphological alterations rather than definitive evidence of improved muscle structure. In addition, both quadriceps wet weight and the wet weight-to-body weight ratio were significantly lower in the HFD group than in the CON group and significantly higher in the HFDR group than in the HFD group. However, myofibre cross-sectional area distribution, fibre-type composition and contractile performance were not assessed. Therefore, the functional significance of the observed morphological changes remains uncertain.

Because resveratrol administration was initiated concurrently with HFD feeding, the present design evaluates whether resveratrol modifies the development of HFD-associated skeletal muscle alterations rather than whether it reverses established pathology. Accordingly, these findings should not be interpreted as evidence of therapeutic reversal.

The present study further showed that the HFD group had increased skeletal muscle levels of TGF-β1, TNF-α, IL-6, $H_2O_2$ and MDA, together with reduced IL-10 levels, SOD activity and T-AOC, indicating that HFD feeding induced local inflammation and disrupted redox homeostasis in skeletal muscle. Previous studies indicate that HFD feeding promotes lipid-associated metabolic stress, chronic inflammation and oxidative stress in skeletal muscle [3,4,41–44]. These processes can interact bidirectionally, with ROS promoting inflammatory signalling and inflammatory mediators further impairing redox ho-

meostasis. Compared with the HFD group, the HFDR group receiving concurrent resveratrol intervention showed significantly lower $H_2O_2$ and MDA levels and higher T-AOC, consistent with a more favourable oxidative stress-related profile under HFD conditions. Previous studies have linked resveratrol to enhanced antioxidant defence and reduced ROS accumulation, including through Nrf2–Keap1-related mechanisms [17,45,46]. However, SOD activity did not differ significantly between the HFDR and HFD groups, indicating that the observed redox changes were not accompanied by increased SOD activity. Although $H_2O_2$ and MDA levels were measured, the mechanisms underlying changes in ROS production, lipid peroxidation and other antioxidant systems were not directly investigated in the present study. As T-AOC reflects overall antioxidant capacity, changes in T-AOC should not be regarded as equivalent to changes in any single antioxidant enzyme. In addition to oxidative stress, resveratrol also showed selective effects on inflammatory indices. The HFDR group exhibited increased IL-10 and reduced TGF-β1 levels, whereas TNF-$\alpha$ and IL-6 were not significantly altered relative to the HFD group. These findings indicate that, under the 5-week intervention conditions used in the present study, concurrent resveratrol intervention was associated with selective differences in inflammation-related indices rather than a broad normalisation of the inflammatory profile associated with HFD feeding. Previous studies have shown that the effects of resveratrol on inflammatory factors such as TNF-$\alpha$ are strongly dependent on dose, tissue type and disease model [39]. Notably, TGF-β1 is involved not only in inflammatory regulation but also in fibroblast activation, collagen deposition and extracellular matrix (ECM) remodelling [47]. In the present study, lower TGF-β1 levels in the HFDR group occurred alongside enrichment of collagen fibril organisation and extracellular matrix organisation among the exploratory candidate genes, suggesting an association between changes in inflammatory status and ECM-related transcriptional responses. Although hydroxyproline content and several ECM-related regulatory proteins were measured, TGF-β/Smad signalling activity, histological collagen deposition and the protein abundance of individual transcriptomic candidates were not directly assessed. Therefore, these findings support an association between changes in inflammatory status and ECM-related biochemical and transcriptional responses but do not establish structural ECM remodelling or a direct causal relationship. Although pathways such as Nrf2-Keap1 and TGF-β/Smad have been implicated in resveratrol-related antioxidant, inflammatory and ECM responses in previous studies, the activation status of these signalling pathways was not directly assessed in the present study.

The exploratory transcriptomic analysis further identified 112 candidate genes showing opposite expression directions between HFD feeding and resveratrol intervention. Importantly, the term "directionally reversed" in the present study denotes opposite expression directions between the HFD versus CON and HFDR versus HFD comparisons and should not be interpreted as complete restoration of gene expression to control levels. In the additional HFDR versus CON analysis, 107 of the 112 exploratory candidates were not significantly different from CON after multiple-testing correction, whereas five remained significantly different. However, particularly given the limited RNA-seq sample size, a non-significant difference does not demonstrate statistical equivalence or biological normalisation. Descriptive recovery analysis indicated that most candidates showed a smaller absolute deviation from the CON mean in HFDR than in HFD, but the magnitude of recovery varied among genes. Therefore, these results support the interpretation of resveratrol-associated opposite-direction transcriptional responses rather than confirmed restoration of the HFD-altered transcriptome. Exploratory GO enrichment analysis highlighted collagen fibril organisation and extracellular matrix organisation among the 112 candidate genes, supporting ECM-related transcriptional responses as a prominent fea-

ture of the exploratory candidate set. Skeletal muscle ECM not only maintains tissue structural integrity but also participates in mechanical force transmission, cell adhesion and regulation of the muscle stem-cell niche [13,48]. Under conditions of obesity and nutrient excess, abnormal collagen deposition and dysregulated ECM turnover can reduce tissue adaptability and impair muscle repair and regeneration [11,49,50]. In the present study, enrichment of ECM-related processes among the exploratory candidate genes occurred alongside changes in muscle fibre morphology and ECM-related biochemical indices. Compared with the CON group, the HFD group showed increased skeletal muscle hydroxyproline content, elevated LOX, MMP-2 and MMP-9 concentrations, reduced TIMP-1 and TIMP-2 concentrations, and higher MMP-2/TIMP-2 and MMP-9/TIMP-1 ratios. Concurrent resveratrol intervention attenuated these changes. Hydroxyproline provides an indirect estimate of collagen content, whereas LOX and MMP/TIMP concentrations reflect biochemical features associated with collagen cross-linking and matrix regulation. However, these measurements do not directly quantify histological collagen deposition, collagen cross-linking or ECM turnover activity. Accordingly, the biochemical findings provide complementary evidence of ECM-related alterations alongside the observed transcriptional responses. PPI network analysis showed that Col3a1, Fbn1, Col5a2, Timp1, Col6a1 and Postn had relatively high network connectivity, whereas Col6a2 was located within the ECM-related interaction subnetwork. Importantly, node degree reflects connectivity within the STRING-derived network under the specified confidence threshold and does not establish regulatory hierarchy, causal importance or direct molecular targeting by resveratrol. Accordingly, these highly connected genes should be regarded as candidate network-associated genes rather than principal regulators of the resveratrol response. Previous studies have implicated Postn, Fbn1 and collagen VI in ECM organisation, matrix remodelling and skeletal muscle regeneration [51–54]. However, their altered expression in the present study does not establish them as direct molecular targets of resveratrol. Notably, the significantly enriched KEGG pathway for protein digestion and absorption may have been driven partly by shared collagen- and ECM-related genes. Its enrichment may therefore reflect ECM-associated molecular characteristics rather than a direct alteration in digestive function. Protein-level and collagen-specific analyses will be required to determine whether these transcriptional changes correspond to structural ECM alterations.

RT-qPCR and RNA-seq showed the same direction of expression change for each of the five selected genes within the HFD versus CON and HFDR versus HFD comparisons. However, Actc1 was downregulated in both comparisons and therefore did not exhibit a directionally reversed expression pattern. Actc1 was included as a representative muscle structural/contractile-related gene rather than as a directionally reversed candidate gene. Exploratory cross-gene regressions between RNA-seq- and RT-qPCR-derived $\log_2$ fold changes did not reach statistical significance in either comparison. Given the small number of genes examined (n = 5), the RT-qPCR results should be interpreted as descriptive support for expression direction rather than quantitative validation of the RNA-seq results. The additional ECM-related biochemical measurements provide complementary evidence of matrix-associated alterations in quadriceps muscle. However, changes in hydroxyproline content and ECM regulatory protein concentrations do not constitute direct protein-level validation of specific transcriptomic candidates, including Col3a1, Fbn1, Postn and Col6a2. Moreover, mRNA changes do not establish corresponding changes in protein abundance or biological function [55,56]. Accordingly, Fbn1, Postn, Myoc and Col6a2 should be regarded as transcriptomic candidate genes whose biological significance requires confirmation at the protein and functional levels. The present findings do not establish Fbn1, Postn or Col6a2 as direct targets of resveratrol, but rather suggest that these genes form part of an ECM-related transcriptional network altered by HFD feeding

and associated with resveratrol intervention. Taken together, the histological, biochemical and transcriptomic findings indicate that concurrent resveratrol intervention was associated with alterations in skeletal muscle morphology, selective changes in inflammatory and oxidative stress-related status, and ECM-related biochemical and transcriptional responses under HFD conditions. Nevertheless, several limitations should be considered.

Only a single resveratrol dose and a 5-week intervention were investigated, limiting assessment of dose–response and time-dependent effects. Only female rats were included in the present study, and sex was therefore not evaluated as an experimental factor. Sex-related hormonal and metabolic differences may influence skeletal muscle responses to HFD and resveratrol; accordingly, the present findings should not be directly extrapolated to males. Future studies including both sexes will be required to determine whether the observed skeletal muscle responses are sex-dependent. The relatively high resveratrol dose used in the present rodent model should not be directly extrapolated to humans. Oral resveratrol undergoes extensive metabolism, and unchanged resveratrol has low systemic bioavailability in humans [57]. Therefore, the present dose should be regarded as an experimental rodent dose rather than a directly translatable human intake. Histological examination used nine biological replicates per group, while RNA-seq and RT-qPCR used three, which may limit the statistical power of transcriptomic analyses. Although quadriceps wet weight and the wet weight to body weight ratio were measured, we did not assess myofibre cross- sectional area distribution, fibre-type composition, muscle strength, endurance or contractile function. Thus, the observed morphological changes cannot be taken as definitive evidence of improved skeletal muscle structure or function. We quantified hydroxyproline by colorimetry and LOX, MMP-2, MMP-9, TIMP-1 and TIMP-2 by ELISA, but lacked collagen-specific histological staining (e.g., Picrosirius Red) and protein validation of individual transcriptomic candidates. Accordingly, we cannot confirm whether altered candidate gene expression translates to corresponding protein changes or assign the detected ECM biochemical shifts to any single candidate gene. While this study used a controlled dietary intervention, we did not dissect the mechanistic connections between inflammation, ECM-associated biochemical and transcriptional changes, and muscle morphology; hence, causal relationships cannot be inferred. Future mechanistic work with pathway-targeted interventions and candidate gene manipulation is needed to establish causality. Follow-up studies should include larger cohorts, both sexes, dose and time response designs, myofibre morphometry, fibre-type profiling, direct muscle functional testing, collagen-specific staining, and protein validation of selected ECM candidates..

## 5. Conclusions

The present study showed that concurrent resveratrol intervention in rats fed a high-fat diet (HFD) was associated with alterations in quadriceps muscle morphology, selective differences in local inflammatory and oxidative stress-related indices (lower TGF-β1, $H_2O_2$ and MDA; higher IL-10 and T-AOC) and reversal of ECM-related indices, without a significant change in total body weight gain. Resveratrol attenuated the HFD-induced increases in hydroxyproline, LOX, MMP-2 and MMP-9, and in the MMP-2/TIMP-2 and MMP-9/TIMP-1 ratios, and increased TIMP-1 and TIMP-2. Exploratory transcriptomic analysis identified 112 candidate genes with opposite expression directions between HFD feeding and resveratrol intervention, of which only five met the FDR and fold-change criteria in both comparisons; GO enrichment highlighted collagen fibril organisation and extracellular matrix organisation, and RT-qPCR showed concordant fold-change directions for the selected genes. These findings support an association between concurrent resvera-

trol intervention and ECM-related transcription. Because muscle function was not assessed and resveratrol was administered concurrently with HFD feeding, functional benefits and reversal of established skeletal muscle abnormalities cannot be inferred.

**Supplementary Materials:** The following supporting information can be downloaded at: https://www.mdpi.com/article/10.3390/cells15232177/s1, Figure S1. Left quadriceps wet weight and wet weight-to-body weight ratio in rats fed a standard or high-fat diet with or without resveratrol supplementation. Figure S2: Quality assessment and gene expression distribution of RNA-seq data from rat quadriceps muscle; Figure S3: Principal component and sample correlation analyses of quadriceps muscle RNA-seq profiles; Figure S4: Gene Ontology enrichment analysis of directionally reversed genes in rat quadriceps muscle following resveratrol intervention; Figure S5: Protein–protein interaction network characteristics of directionally reversed genes and extracellular matrix-related candidate genes; Figure S6: Exploratory cross-gene regression between RNA-seq- and RT-qPCR-derived $\log_2$ fold changes for selected genes; Table S1: Primer sequences used for RT-qPCR assessment of selected RNA-seq expression trends; Table S2: FDR re-evaluation of the 112 exploratory candidate genes showing opposite expression directions between HFD feeding and resveratrol intervention; Table S3: Expression status and descriptive recovery metrics of the 112 exploratory candidate genes relative to the CON group; Table S4: Sensitivity analysis of the PPI network under different STRING combined-score thresholds; Table S5: Macronutrient composition and energy density of the standard and high-fat diets; Table S6: Two-way ANOVA results for the effects of diet and resveratrol on body weight gain, skeletal muscle histomorphological indices, and inflammatory and oxidative stress-related indices.

**Author Contributions:** Conceptualisation: H.Z. (Huibin Zhang), L.X. (Lei Xu), and X.Z. (Xiaodong Zhang); methodology: H.Z. (Huibin Zhang), Q.L. (Qinggang Li), and Z.Y. (Zongjun Yin); validation: Q.L. (Qian Li), X.D. (Xinyi Du), and H.Z. (Honglong Zhu); formal analysis: H.Z. (Huibin Zhang), W.L. (Wenxi Li), and X.Z. (Xiaodong Zhang); investigation: H.Z. (Huibin Zhang), Q.L. (Qian Li), W.L. (Wenxi Li), and H.J. (Hai Jin); resources: Z.Y. (Zongjun Yin) and L.X. (Lei Xu); data curation: W.L. (Wenxi Li), S.Z. (Shuanping Zhao), and Z.Y. (Zongjun Yin); writing—original draft preparation: H.Z. (Huibin Zhang) and W.L. (Wenxi Li); writing—review and editing: X.Z. (Xiaodong Zhang) and L.X. (Lei Xu); visualisation: W.L. (Wenxi Li); supervision: X.Z. (Xiaodong Zhang) and L.X. (Lei Xu); project administration: L.X. (Lei Xu); funding acquisition: L.X. (Lei Xu). All authors have read and agreed to the published version of the manuscript.

**Funding:** Project of Beef Cattle Revitalization of Anhui Provincial Science and Technology Department, 02513b10050018; Anhui Provincial Science and Technology Innovation Breakthrough Project (Major Project), 202423m10050001; Anhui Provincial Science and Technology Innovation Breakthrough Project (Major Project), XJBS-202432; Young Talent Program of Anhui Academy of Agricultural Sciences, QNYC-202221.

**Institutional Review Board Statement:** The animal study protocol was approved by the Institutional Animal Care and Use Committee of Anhui Agricultural University (Approval No. AHAU2023–002; Approval Date: 24 February 2023). All procedures were conducted in accordance with institutional guidelines for the care and use of laboratory animals.

**Informed Consent Statement:** Not applicable.

**Data Availability Statement:** The RNA-seq datasets generated in this study have been deposited in the China National Center for Bioinformation (CNCB) database under accession number OMIX020685 and are publicly available at: https://ngdc.cncb.ac.cn/omix/preview/tQUUeolKrz (accessed on 25 November 2026). Other data supporting the findings of this study are available from the corresponding author upon reasonable request.

**Conflicts of Interest:** The authors declare no conflicts of interest.

## References


1. Pileggi, C.A.; Hooks, B.G.; McPherson, R.; Dent, R.R.M.; Harper, M.E. Targeting skeletal muscle mitochondrial health in obesity. *Clin. Sci.* **2022**, *136*, 1081–1110. https://doi.org/10.1042/cs20210506.
2. Samuel, V.T.; Shulman, G.I. Mechanisms for insulin resistance: Common threads and missing links. *Cell* **2012**, *148*, 852–871. https://doi.org/10.1016/j.cell.2012.02.017.
3. Fritzen, A.M.; Lundsgaard, A.M.; Kiens, B. Tuning fatty acid oxidation in skeletal muscle with dietary fat and exercise. *Nat. Rev. Endocrinol.* **2020**, *16*, 683–696. https://doi.org/10.1038/s41574-020-0405-1.
4. Turner, N.; Cooney, G.J.; Kraegen, E.W.; Bruce, C.R. Fatty acid metabolism, energy expenditure and insulin resistance in muscle. *J. Endocrinol.* **2014**, *220*, T61–T79. https://doi.org/10.1530/joe-13-0397.
5. Imierska, M.; Zabielski, P.; Roszczyc-Owsiejczuk, K.; Sokołowska, E.; Pogodzińska, K.; Kojta, I.; Błachnio-Zabielska, A. Serine Palmitoyltransferase Gene Silencing Prevents Ceramide Accumulation and Insulin Resistance in Muscles in Mice Fed a High-Fat Diet. *Cells* **2022**, *11*, 1123. https://doi.org/10.3390/cells11071123.
6. Lee, H.; Ha, T.Y.; Jung, C.H.; Nirmala, F.S.; Park, S.Y.; Huh, Y.H.; Ahn, J. Mitochondrial dysfunction in skeletal muscle contributes to the development of acute insulin resistance in mice. *J. Cachexia Sarcopenia Muscle* **2021**, *12*, 1925–1939. https://doi.org/10.1002/jcsm.12794.
7. Heo, J.W.; No, M.H.; Cho, J.; Choi, Y.; Cho, E.J.; Park, D.H.; Kim, T.W.; Kim, C.J.; Seo, D.Y.; Han, J.; et al. Moderate aerobic exercise training ameliorates impairment of mitochondrial function and dynamics in skeletal muscle of high-fat diet-induced obese mice. *Faseb j.* **2021**, *35*, e21340. https://doi.org/10.1096/fj.202002394R.
8. Toniolo, L.; Concato, M.; Giacomello, E. Resveratrol, a Multitasking Molecule That Improves Skeletal Muscle Health. *Nutrients* **2023**, *15*, 3413. https://doi.org/10.3390/nu15153413.
9. Biswas, S.K. Does the Interdependence between Oxidative Stress and Inflammation Explain the Antioxidant Paradox? *Oxid. Med. Cell Longev.* **2016**, *2016*, 5698931. https://doi.org/10.1155/2016/5698931.
10. Russell-Guzmán, J.; Américo-Da Silva, L.; Cadagan, C.; Maturana, M.; Palomero, J.; Estrada, M.; Barrientos, G.; Buvinic, S.; Hidalgo, C.; Llanos, P. Activation of the ROS/TXNIP/NLRP3 pathway disrupts insulin-dependent glucose uptake in skeletal muscle of insulin-resistant obese mice. *Free Radic. Biol. Med.* **2024**, *222*, 187–198. https://doi.org/10.1016/j.freeradbiomed.2024.06.011.
11. Li, Y.; Guo, W.; Li, H.; Wang, Y.; Liu, X.; Kong, W. The Change of Skeletal Muscle Caused by Inflammation in Obesity as the Key Path to Fibrosis: Thoughts on Mechanisms and Intervention Strategies. *Biomolecules* **2024**, *15*, 20. https://doi.org/10.3390/biom15010020.
12. Ong, C.H.; Tham, C.L.; Harith, H.H.; Firdaus, N.; Israf, D.A. TGF-β-induced fibrosis: A review on the underlying mechanism and potential therapeutic strategies. *Eur. J. Pharmacol.* **2021**, *911*, 174510. https://doi.org/10.1016/j.ejphar.2021.174510.
13. Gillies, A.R.; Lieber, R.L. Structure and function of the skeletal muscle extracellular matrix. *Muscle Nerve* **2011**, *44*, 318–331. https://doi.org/10.1002/mus.22094.
14. Xu, Y.; Fang, M.; Li, X.; Wang, D.; Yu, L.; Ma, F.; Jiang, J.; Zhang, L.; Li, P. Contributions of Common Foods to Resveratrol Intake in the Chinese Diet. *Foods* **2024**, *13*, 1267.
15. Baur, J.A.; Sinclair, D.A. Therapeutic potential of resveratrol: The in vivo evidence. *Nat. Rev. Drug Discov.* **2006**, *5*, 493–506. https://doi.org/10.1038/nrd2060.
16. Long, Y.; Wu, Y.; Zhong, Y.; Wu, Y.; Ye, H.; Luo, Y.; Xiao, L.; Ma, Y.; Wang, M. Resveratrol as a potential therapeutic agent for sarcopenic obesity: Insights from in vivoperiments. *Biomed. Pharmacother.* **2024**, *179*, 117396. https://doi.org/10.1016/j.biopha.2024.117396.
17. Shabani, M.; Hosseini, H.; Tajik, M.H.; Meshkani, R.; Sadeghi, A. Resveratrol relieves HFD-induced insulin resistance in skeletal muscle tissue through antioxidant capacity enhancement and the Nrf2-Keap1 signaling pathway. *Mol. Biol. Rep.* **2024**, *51*, 516. https://doi.org/10.1007/s11033-024-09434-4.
18. Pan, X.; Xue, G.; Zhao, M.; Xiang, Z.; Liu, D.; Duan, Z.; Wang, C. Resveratrol ameliorates high-fat diet-induced insulin resistance via the DDIT4/mTOR pathway in skeletal muscle. *Biomed. Rep.* **2025**, *22*, 99. https://doi.org/10.3892/br.2025.1977.
19. Hyatt, J.K.; de Cabo, R.; Mattison, J.A. Resveratrol Blunts Mitochondrial Loss in Slow and Mixed Skeletal Muscle Phenotypes of Non-Human Primates following a Long-Term High Fat/Sugar Diet. *J. Diet. Suppl.* **2023**, *20*, 563–581. https://doi.org/10.1080/19390211.2022.2039340.
20. Lagouge, M.; Argmann, C.; Gerhart-Hines, Z.; Meziane, H.; Lerin, C.; Daussin, F.; Messadeq, N.; Milne, J.; Lambert, P.; Elliott, P.; et al. Resveratrol improves mitochondrial function and protects against metabolic disease by activating SIRT1 and PGC-1alpha. *Cell* **2006**, *127*, 1109–1122. https://doi.org/10.1016/j.cell.2006.11.013.

21. Zhu, C.; Zhang, H.; Dai, Z.; Liao, Z.; Tian, F.; Fan, S.; Li, W.; Li, Y.; Zheng, X.; Yin, Z.; et al. Resveratrol ameliorates High-Fat Diet induced ovarian damage by reshaping gut microbiota and reversing aberrant ovarian energy metabolism and gene expression. *Food Res. Int.* **2026**, *242*, 120056. https://doi.org/10.1016/j.foodres.2026.120056.
22. Moriggi, M.; Belloli, S.; Barbacini, P.; Murtaj, V.; Torretta, E.; Chaabane, L.; Canu, T.; Penati, S.; Malosio, M.L.; Esposito, A.; et al. Skeletal Muscle Proteomic Profile Revealed Gender-Related Metabolic Responses in a Diet-Induced Obesity Animal Model. *Int. J. Mol. Sci.* **2021**, *22*, 4680. https://doi.org/10.3390/ijms22094680.
23. Toniolo, L.; Gazzin, S.; Rosso, N.; Giraudi, P.; Bonazza, D.; Concato, M.; Zanconati, F.; Tiribelli, C.; Giacomello, E. Gender Differences in the Impact of a High-Fat, High-Sugar Diet in Skeletal Muscles of Young Female and Male Mice. *Nutrients* **2024**, *16*, 1467. https://doi.org/10.3390/nu16101467.
24. Shelley, S.P.; James, R.S.; Eustace, S.J.; Turner, M.C.; Brett, R.; Eyre, E.L.J.; Tallis, J. Adverse effects of high-fat diet consumption on contractile mechanics of isolated mouse skeletal muscle are reduced when supplemented with resveratrol. *J. Physiol.* **2025**, *603*, 2675–2698. https://doi.org/10.1113/jp287056.
25. Wenzel, E.; Soldo, T.; Erbersdobler, H.; Somoza, V. Bioactivity and metabolism of trans-resveratrol orally administered to Wistar rats. *Mol. Nutr. Food Res.* **2005**, *49*, 482–494. https://doi.org/10.1002/mnfr.200500003.
26. Crowell, J.A.; Korytko, P.J.; Morrissey, R.L.; Booth, T.D.; Levine, B.S. Resveratrol-associated renal toxicity. *Toxicol. Sci.* **2004**, *82*, 614–619. https://doi.org/10.1093/toxsci/kfh263.
27. Wang, P.; Ma, Y.; Wang, D.; Zhao, W.; Hu, X.; Chen, F.; Zhao, X. Protective Effects of Dietary Resveratrol against Chronic Low-Grade Inflammation Mediated through the Gut Microbiota in High-Fat Diet Mice. *Nutrients* **2022**, *14*, 1994. https://doi.org/10.3390/nu14101994.
28. Schneider, C.A.; Rasband, W.S.; Eliceiri, K.W. NIH Image to ImageJ: 25 years of image analysis. *Nat. Methods* **2012**, *9*, 671–675. https://doi.org/10.1038/nmeth.2089.
29. Kim, D.; Paggi, J.M.; Park, C.; Bennett, C.; Salzberg, S.L. Graph-based genome alignment and genotyping with HISAT2 and HISAT-genotype. *Nat. Biotechnol.* **2019**, *37*, 907–915. https://doi.org/10.1038/s41587-019-0201-4.
30. Liao, Y.; Smyth, G.K.; Shi, W. featureCounts: An efficient general purpose program for assigning sequence reads to genomic features. *Bioinformatics* **2014**, *30*, 923–930. https://doi.org/10.1093/bioinformatics/btt656.
31. Love, M.I.; Huber, W.; Anders, S. Moderated estimation of fold change and dispersion for RNA-seq data with DESeq2. *Genome Biol.* **2014**, *15*, 550. https://doi.org/10.1186/s13059-014-0550-8.
32. Yu, G.; Wang, L.G.; Han, Y.; He, Q.Y. clusterProfiler: An R package for comparing biological themes among gene clusters. *Omics* **2012**, *16*, 284–287. https://doi.org/10.1089/omi.2011.0118.
33. Szklarczyk, D.; Kirsch, R.; Koutrouli, M.; Nastou, K.; Mehryary, F.; Hachilif, R.; Gable, A.L.; Fang, T.; Doncheva, N.T.; Pyysalo, S.; et al. The STRING database in 2023: Protein-protein association networks and functional enrichment analyses for any sequenced genome of interest. *Nucleic Acids Res.* **2023**, *51*, D638–D646. https://doi.org/10.1093/nar/gkac1000.
34. Bustin, S.A.; Benes, V.; Garson, J.A.; Hellemans, J.; Huggett, J.; Kubista, M.; Mueller, R.; Nolan, T.; Pfaffl, M.W.; Shipley, G.L.; et al. The MIQE guidelines: Minimum information for publication of quantitative real-time PCR experiments. *Clin. Chem.* **2009**, *55*, 611–622. https://doi.org/10.1373/clinchem.2008.112797.
35. Boutilier, J.K.; Taylor, R.L.; Ram, R.; McNamara, E.; Nguyen, Q.; Goullée, H.; Chandler, D.; Mehta, M.; Balmer, L.; Laing, N.G.; et al. Variable cardiac $\alpha$-actin (Actc1) expression in early adult skeletal muscle correlates with promoter methylation. *Biochim. Biophys. Acta Gene Regul. Mech.* **2017**, *1860*, 1025–1036. https://doi.org/10.1016/j.bbagrm.2017.08.004.
36. Ochala, J.; Iwamoto, H.; Ravenscroft, G.; Laing, N.G.; Nowak, K.J. Skeletal and cardiac $\alpha$-actin isoforms differently modulate myosin cross-bridge formation and myofibre force production. *Hum. Mol. Genet.* **2013**, *22*, 4398–4404. https://doi.org/10.1093/hmg/ddt289.
37. Livak, K.J.; Schmittgen, T.D. Analysis of relative gene expression data using real-time quantitative PCR and the $2^{-\Delta\Delta C_T}$ Method. *Methods* **2001**, *25*, 402–408. https://doi.org/10.1006/meth.2001.1262.
38. Baur, J.A.; Pearson, K.J.; Price, N.L.; Jamieson, H.A.; Lerin, C.; Kalra, A.; Prabhu, V.V.; Allard, J.S.; Lopez-Lluch, G.; Lewis, K.; et al. Resveratrol improves health and survival of mice on a high-calorie diet. *Nature* **2006**, *444*, 337–342. https://doi.org/10.1038/nature05354.
39. Szkudelski, T.; Szkudelska, K. Resveratrol and diabetes: From animal to human studies. *Biochim. Biophys. Acta* **2015**, *1852*, 1145–1154. https://doi.org/10.1016/j.bbadis.2014.10.013.
40. Zheng, J.; Chen, L.L.; Zhang, H.H.; Hu, X.; Kong, W.; Hu, D. Resveratrol improves insulin resistance of catch-up growth by increasing mitochondrial complexes and antioxidant function in skeletal muscle. *Metabolism* **2012**, *61*, 954–965. https://doi.org/10.1016/j.metabol.2011.11.005.

41. Muoio, D.M. Metabolic inflexibility: When mitochondrial indecision leads to metabolic gridlock. *Cell* **2014**, *159*, 1253–1262. https://doi.org/10.1016/j.cell.2014.11.034.
42. Hotamisligil, G.S. Inflammation and metabolic disorders. *Nature* **2006**, *444*, 860–867. https://doi.org/10.1038/nature05485.
43. Reuter, S.; Gupta, S.C.; Chaturvedi, M.M.; Aggarwal, B.B. Oxidative stress, inflammation, and cancer: How are they linked? *Free Radic. Biol. Med.* **2010**, *49*, 1603–1616. https://doi.org/10.1016/j.freeradbiomed.2010.09.006.
44. Furukawa, S.; Fujita, T.; Shimabukuro, M.; Iwaki, M.; Yamada, Y.; Nakajima, Y.; Nakayama, O.; Makishima, M.; Matsuda, M.; Shimomura, I. Increased oxidative stress in obesity and its impact on metabolic syndrome. *J. Clin. Invest.* **2004**, *114*, 1752–1761. https://doi.org/10.1172/jci21625.
45. Zhang, X.; Liu, X.; Wan, F.; You, W.; Tan, X.; Sheng, Q.; Li, C.; Hu, Z.; Liu, G.; Zhao, H. Protective effect of resveratrol against hydrogen peroxide-induced oxidative stress in bovine skeletal muscle cells. *Meat Sci.* **2022**, *185*, 108724. https://doi.org/10.1016/j.meatsci.2021.108724.
46. Haramizu, S.; Asano, S.; Butler, D.C.; Stanton, D.A.; Hajira, A.; Mohamed, J.S.; Alway, S.E. Dietary resveratrol confers apoptotic resistance to oxidative stress in myoblasts. *J. Nutr. Biochem.* **2017**, *50*, 103–115. https://doi.org/10.1016/j.jnutbio.2017.08.008.
47. Wynn, T.A. Cellular and molecular mechanisms of fibrosis. *J. Pathol.* **2008**, *214*, 199–210. https://doi.org/10.1002/path.2277.
48. Zhang, W.; Liu, Y.; Zhang, H. Extracellular matrix: An important regulator of cell functions and skeletal muscle development. *Cell Biosci.* **2021**, *11*, 65. https://doi.org/10.1186/s13578-021-00579-4.
49. Musale, V.; Wasserman, D.H.; Kang, L. Extracellular matrix remodelling in obesity and metabolic disorders. *Life Metab.* **2023**, *2*, load021. https://doi.org/10.1093/lifemeta/load021.
50. Uezumi, A.; Ito, T.; Morikawa, D.; Shimizu, N.; Yoneda, T.; Segawa, M.; Yamaguchi, M.; Ogawa, R.; Matev, M.M.; Miyagoe-Suzuki, Y.; et al. Fibrosis and adipogenesis originate from a common mesenchymal progenitor in skeletal muscle. *J. Cell Sci.* **2011**, *124*, 3654–3664. https://doi.org/10.1242/jcs.086629.
51. Urciuolo, A.; Quarta, M.; Morbidoni, V.; Gattazzo, F.; Molon, S.; Grumati, P.; Montemurro, F.; Tedesco, F.S.; Blaauw, B.; Cossu, G.; et al. Collagen VI regulates satellite cell self-renewal and muscle regeneration. *Nat. Commun.* **2013**, *4*, 1964. https://doi.org/10.1038/ncomms2964.
52. Cescon, M.; Gattazzo, F.; Chen, P.; Bonaldo, P. Collagen VI at a glance. *J. Cell Sci.* **2015**, *128*, 3525–3531. https://doi.org/10.1242/jcs.169748.
53. Ito, N.; Miyagoe-Suzuki, Y.; Takeda, S.; Kudo, A. Periostin Is Required for the Maintenance of Muscle Fibers during Muscle Regeneration. *Int. J. Mol. Sci.* **2021**, *22*, 3627. https://doi.org/10.3390/ijms22073627.
54. Li, L.; Huang, J.; Liu, Y. The extracellular matrix glycoprotein fibrillin-1 in health and disease. *Front. Cell Dev. Biol.* **2023**, *11*, 1302285. https://doi.org/10.3389/fcell.2023.1302285.
55. Liu, Y.; Beyer, A.; Aebersold, R. On the Dependency of Cellular Protein Levels on mRNA Abundance. *Cell* **2016**, *165*, 535–550. https://doi.org/10.1016/j.cell.2016.03.014.
56. Vogel, C.; Marcotte, E.M. Insights into the regulation of protein abundance from proteomic and transcriptomic analyses. *Nat. Rev. Genet.* **2012**, *13*, 227–232. https://doi.org/10.1038/nrg3185.
57. Walle, T.; Hsieh, F.; DeLegge, M.H.; Oatis, J.E., Jr.; Walle, U.K. High absorption but very low bioavailability of oral resveratrol in humans. *Drug Metab. Dispos.* **2004**, *32*, 1377–1382. https://doi.org/10.1124/dmd.104.000885.


**Disclaimer/Publisher's Note:** The statements, opinions and data contained in all publications are solely those of the individual author(s) and contributor(s) and not of MDPI and/or the editor(s). MDPI and/or the editor(s) disclaim responsibility for any injury to people or property resulting from any ideas, methods, instructions or products referred to in the content.